Supporting Information

Construction of Symbiotic One-Dimensional Ionic Channels in Cobalt-based Covalent Organic Framework for High-Performance Oxygen Reduction Electrocatalysis

Rong Ren,[a] Liting Yang,[b] Zhang Lin,[a] Xiaoyu Li,[a] Shuomeng Zhang,[a] Tianlong Zheng,[a] Duojie Wu,[c] Jian Wang,[d] Zidong Wei,*[d] Wei Ding,[d] Ning Huang,[b]* Meng Gu [c] and Qinggang He *[ae]

a. College of Chemical and Biological Engineering, Zhejiang University, Hangzhou, Zhejiang 310027, China.
b. MOE Key Laboratory of Macromolecular Synthesis and Functionalization, State Key Laboratory of Silicon Materials, Department of Polymer Science and Engineering, Zhejiang University, Hangzhou 310027, China.
c. Department of Materials Science and Engineering, Southern University of Science and Technology, Shenzhen 518055, China.
d. The State Key Laboratory of Power Transmission Equipment & System Security and New Technology, Chongqing Key Laboratory of Chemical Process for Clean Energy and Resource Utilization, School of Chemistry and Chemical Engineering, Chongqing University, Chongqing 400044, China.
e. Ningbo Research Institute, Zhejiang University, Ningbo, Zhejiang 315100, China

* Corresponding author. E-mail: qghe@zju.edu.cn (Q.H.); nhuang@zju.edu.cn (N. H.); zdwei@cqu.edu.cn (Z. W.)

Materials

Acetic acid, $Co(CH_3COO)_2.4H_2O$, trimethylamine, K_2CO_3, dichlorobenzene, ethanol, isopropanol, and N,N-dimethylformamide (DMF) were purchased from Sinopharm Chemical Reagent Co. Ltd. and used as received. 4-Nitrobenzaldehyde, pyrrole, 2,5-dihydroxyterephthalaldehyde, 2,5-dimethoxyterephthalaldehyde and 1,3-diiodopropane were purchased from Energy Chemical. Tetraphenylaminoporphyrin cobalt and 3-iodo-trimethylpropylaminium iodide were synthesized according to the literature.[1] Argon gas and oxygen gas (99.99%) were purchased from Jingong Special Gas Factory Co., Ltd. Deionized water with a conductivity of 18 MΩ·cm was produced by an SMART ultrapure water system.

Structure and compositional characterization

The molecular structure was identified by ^1H NMR (Mercury Plus 400 NMR spectrometer, Varian) and FTIR (Thermo Fisher Scientific IS5). Transmission electron microscopy (TEM) and high-resolution TEM images were obtained using a Tecnai G2 F30 ST microscope and a Tecnai G2 20 S-twin microscope, respectively. Nitrogen physisorption isotherms were collected on a Belsorp Max II instrument at 77 K. Powder X-ray diffraction (PXRD) measurements were performed on a BRUKER D8-Advance X-ray diffraction system equipped with a Cu sealed tube (λ = 1.54178 Å). XPS measurements were performed on a Thermo Scientific K-Alpha+ instrument with an Al Kα source at 150 W. The powders of the samples were dispersed in ethanol solution and deposited onto silicon wafers. Analysis and quantification of the obtained data were performed using Avantage software. All the binding energies derived from the XPS spectra were calibrated to C 1s at 284.45 eV. Inductively coupled plasma–mass spectrometry (ICP–MS) analysis was performed on an Agilent 720ES instrument to determine the content of Co. The element analysis was performed with a Flash EA 1112 element analyzer (Thermo Finnigan). XAS spectra at the Co K-edge were recorded at room temperature in transmission mode at the BL14W1 beamline of the Shanghai Synchrotron Radiation Facility (SSRF). The energy of the Co K-edge was calibrated

by pure Co foil. All the acquired XAS data were analyzed and processed by the IFEFFIT software packages according to the standard procedures.

Calculation of electrochemical parameters

Electrochemical impedance spectroscopy (EIS) measurements were carried out in 0.1 M KOH at OCP in the frequency range from 100 kHz to 1 Hz.

Identifying the catalytic kinetics of ORR catalysts is of great significance for the recognition of and improvement in catalytic performance. The Tafel plots were obtained through the polarization curves, and the ORR Tafel slope was fitted and calculated according to the Tafel Equation (1):

$$\eta=a+b*\log|j_k| \qquad (1)$$

where η is the overpotential, j_k is the kinetic current density, a is a constant, representing the overpotential at a current density of 1 A/cm^2 and b is the Tafel slope.

After polarization curve measurements were performed at different electrode rotating speeds, the number of electrons transferred (n) per oxygen molecule and kinetic current density (j_k) were calculated by the Koutecky−Levich (K–L) Equation (2):

$$\frac{1}{j}=\frac{1}{j_k}+\frac{1}{j_d}=\frac{1}{j_k}+\frac{1}{0.62nFD_{O_2}^{2/3}v^{-1/6}C_{O_2}\omega^{1/2}} \qquad (2)$$

In the K–L equation, j, j_d, and j_k are the measured current density, limiting current density, and kinetic current density, respectively; ω is the rotation speed in rpm, and n is the number of electrons transferred per oxygen molecule. F is the Faraday constant (96,485 C mol^{-1}), C_0 is the bulk concentration of O_2 (1.2×10^{-6} mol cm^{-3}), D_0 is the diffusion coefficient of O_2 in 0.1 M KOH solution (1.9×10^{-5} cm^2 s^{-1}), and v is the kinematic viscosity (0.01 cm^2 s^{-1}).

The turnover frequency (TOF, number of electrons per Co active site and per second) was calculated according to Equation (3):

$$TOF = \frac{j_k}{\frac{W_{Co}}{M_{Co}} \times N_A \times m_{loading}} = 1.224 \times \frac{|j_k|}{|W_{Co}|}(e^- \cdot site^{-1} \cdot s^{-1}) \quad (3)$$

where W_{Co} and M_{Co} ($|M_{Co}|$=58.93 g mol^{-1}) are the mass fraction and molar weight of Co, respectively. m is catalyst loading on the RDE. W_{Co} is measured from ICP–MS analysis. j_k is the kinetic current density. N_A is Avogadro's number (6.02×10^{23} mol^{-1}).

RRDE tests were performed and the H_2O_2 yield was evaluated using equation (4):

$$H_2O_2 \text{ yield}(\%) = 2 \times \frac{\frac{i_r}{N_C}}{i_d + \frac{i_r}{N_C}} \quad (4)$$

where i_r is ring current, i_d is disk current, and N_C is the collection efficiency of the RRDE, defined as the fraction of the peroxide product from the disk to the ring.

Preparation of catalyst-coated GDE for fuel cell testing

To prepare the electrocatalyst ink, 80 mg of carbon black ECP-600 and 40 mg of cobalt-based composite catalyst (TAPPCo-OMe and TAPPCo-QA were used for different electrode manufacturing) were weighed and placed in a 50 mL centrifuge tube. Subsequently, water/isopropanol (2 mL/18 mL) was slowly added to the tube, and a shearing dispersion procedure was carried out by a high-shear dispersion emulsifier. Thirty milligrams of polyfluorene ionomer was added to the mixed solution with catalysts and ultrasonicated for 1 h to form a uniform ink mixture. The mixture was sprayed onto Toray carbon paper (4 cm^2, TGP-H-60) using a spray gun connected to the nitrogen line to obtain a COF catalyst loading of 3 mg/cm^2. The PtRu/C anode was prepared in a similar manner and reached a metal loading of 1 mg/cm^2.

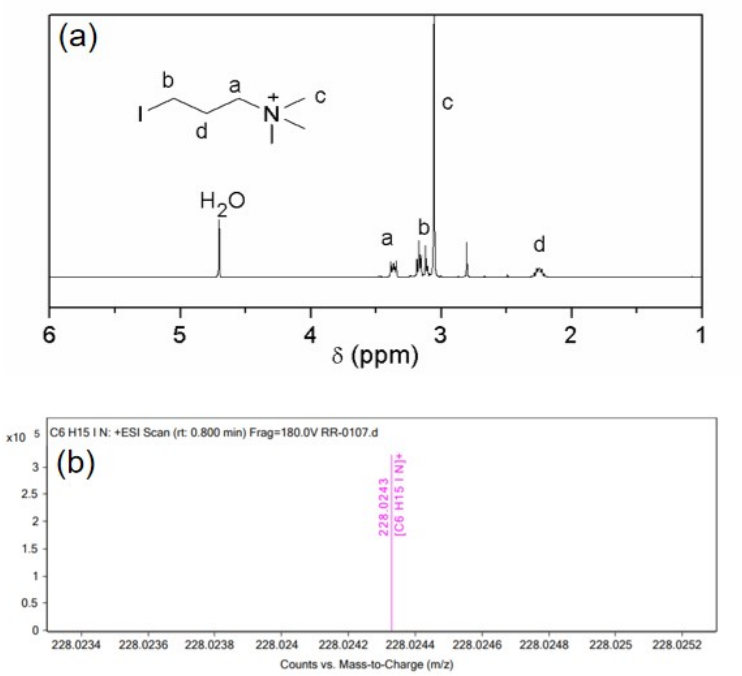

Fig. S1 ^{1}H NMR and mass spectra of ITMPA.

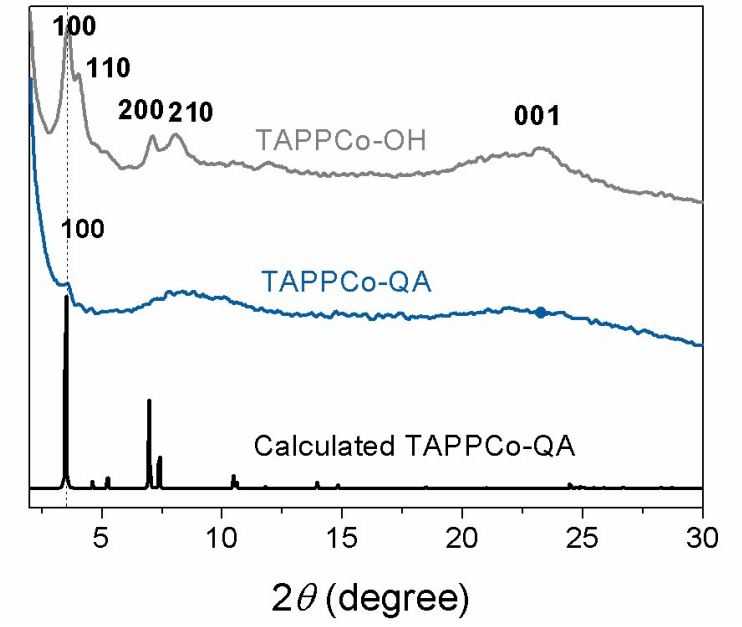

Fig. S2 Experimental and calculated PXRD patterns of TAPPCo-OH and TAPPCo-QA.

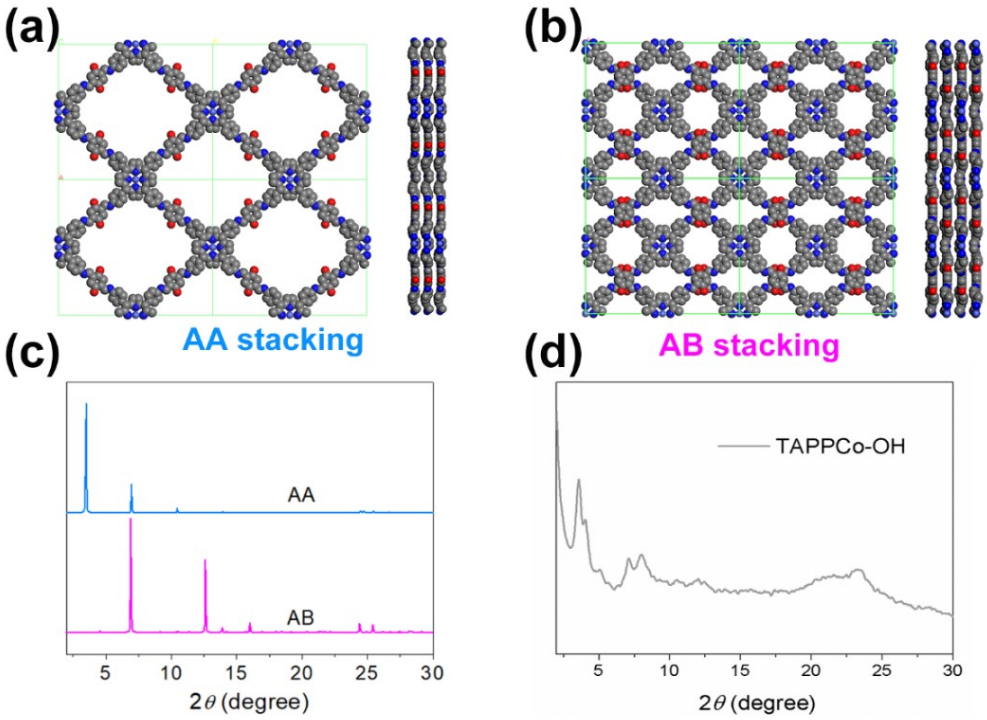

Fig. S3 Theoretical unit-cell structure of the slipped AA-stacking mode (a) and staggered AB-stacking mode (b) of the TAPPCo-OH COF. Calculated PXRD pattern (c) from the proposed models and experimental PXRD pattern (d) of the TAPPCo-OH COF

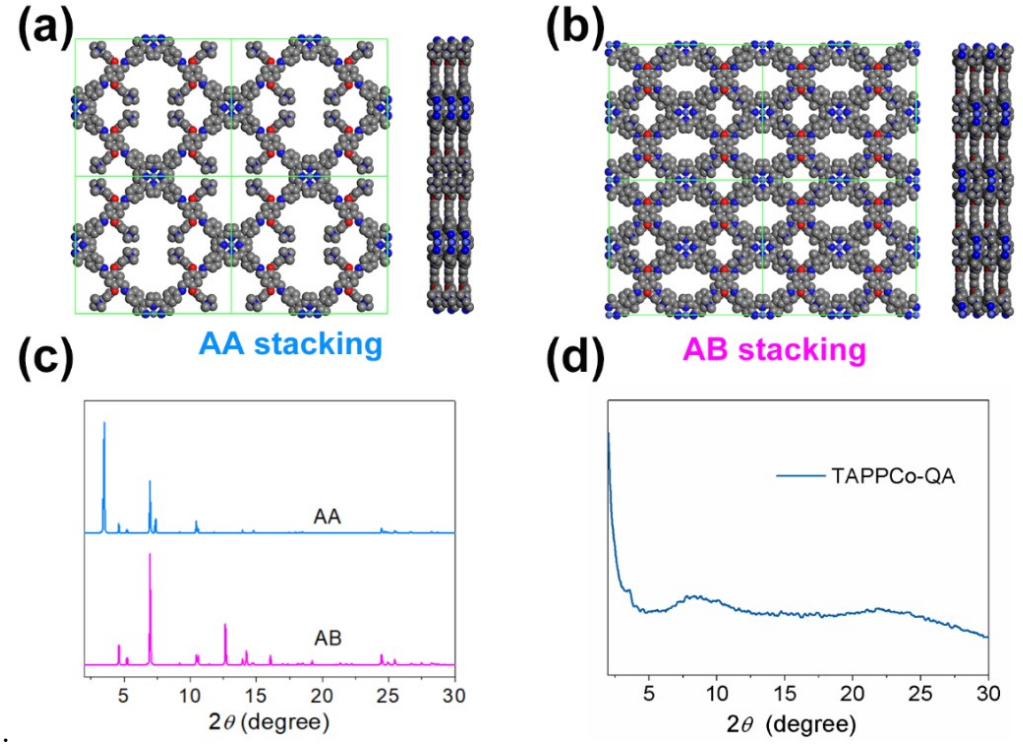

Fig. S4 Theoretical unit-cell structure of the slipped AA-stacking mode (a) and staggered AB-stacking mode (b) of the TAPPCo-QA COF, the calculated PXRD pattern (c) from the proposed models and the experimental PXRD pattern (d) of the TAPPCo-QA COF.

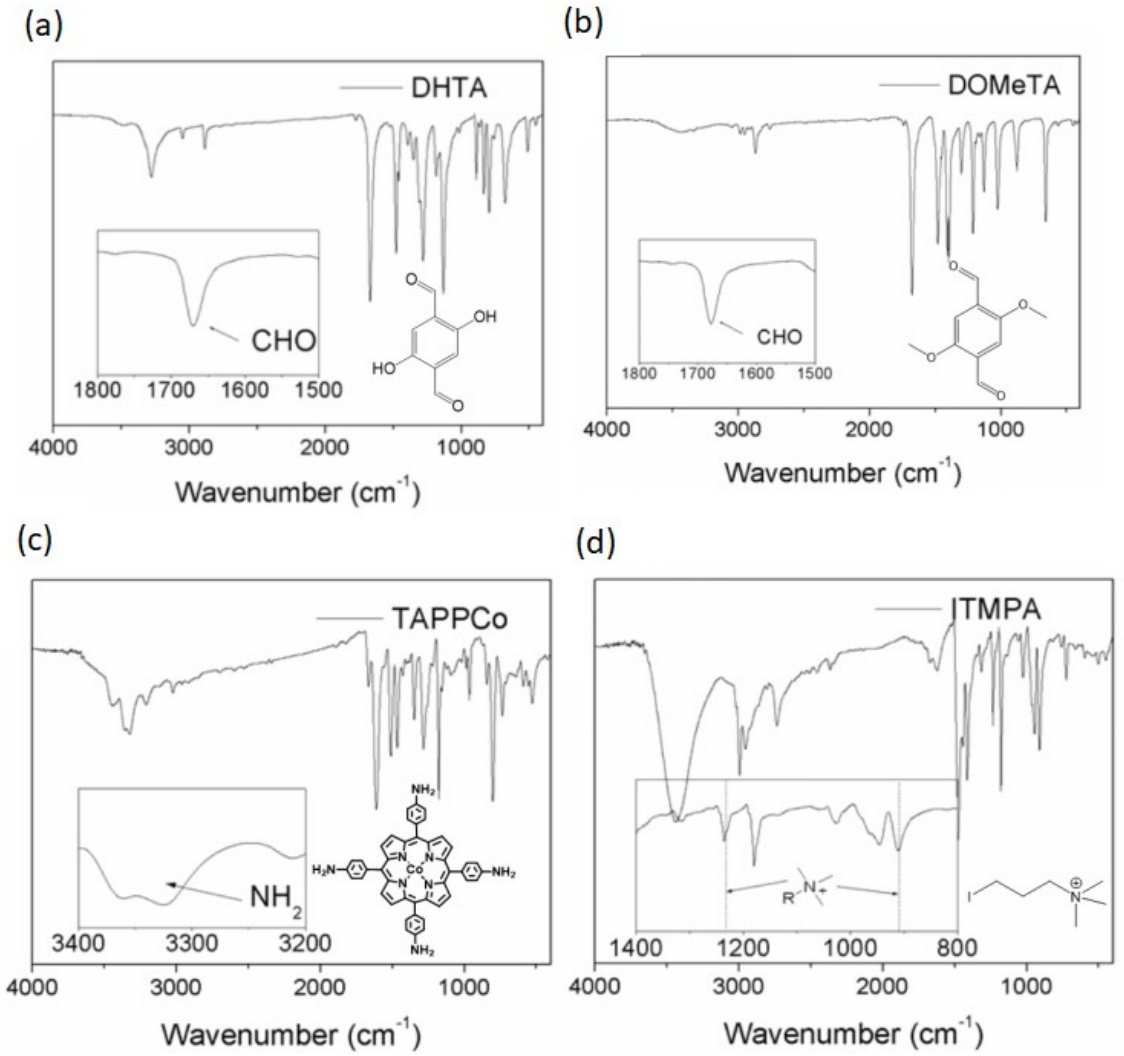

Fig. S5 FTIR spectra of DHTA, DOMeTA, TAPPCo and ITMPA

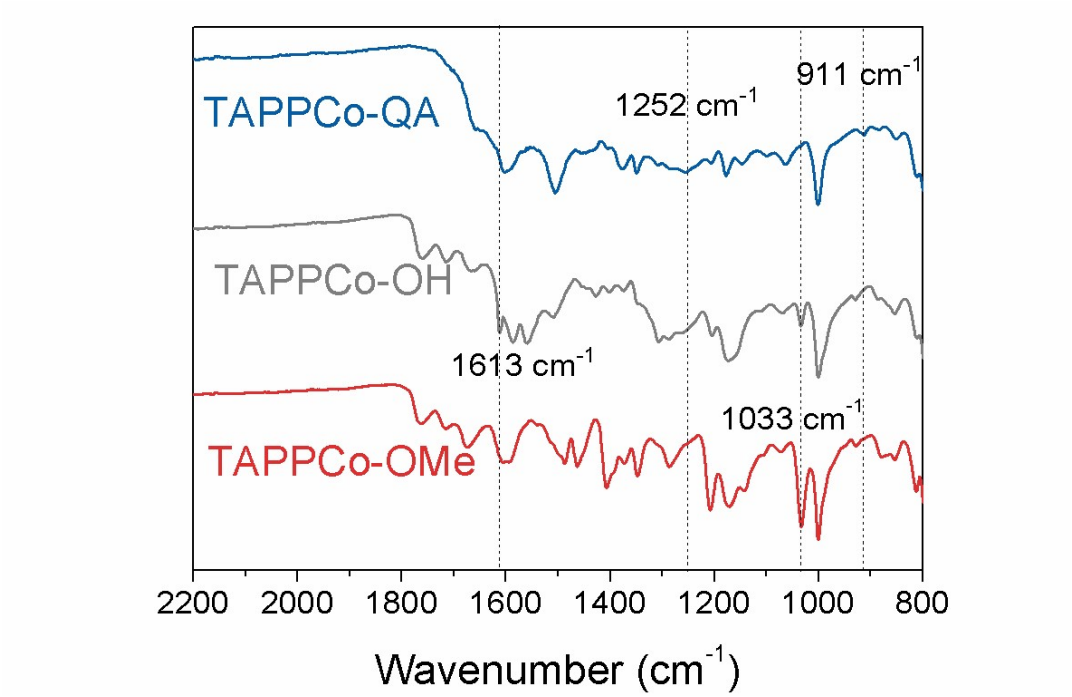

Fig. S6 FTIR spectra of TAPPCo-QA, TAPPCo-OH and TAPPCo-OMe.

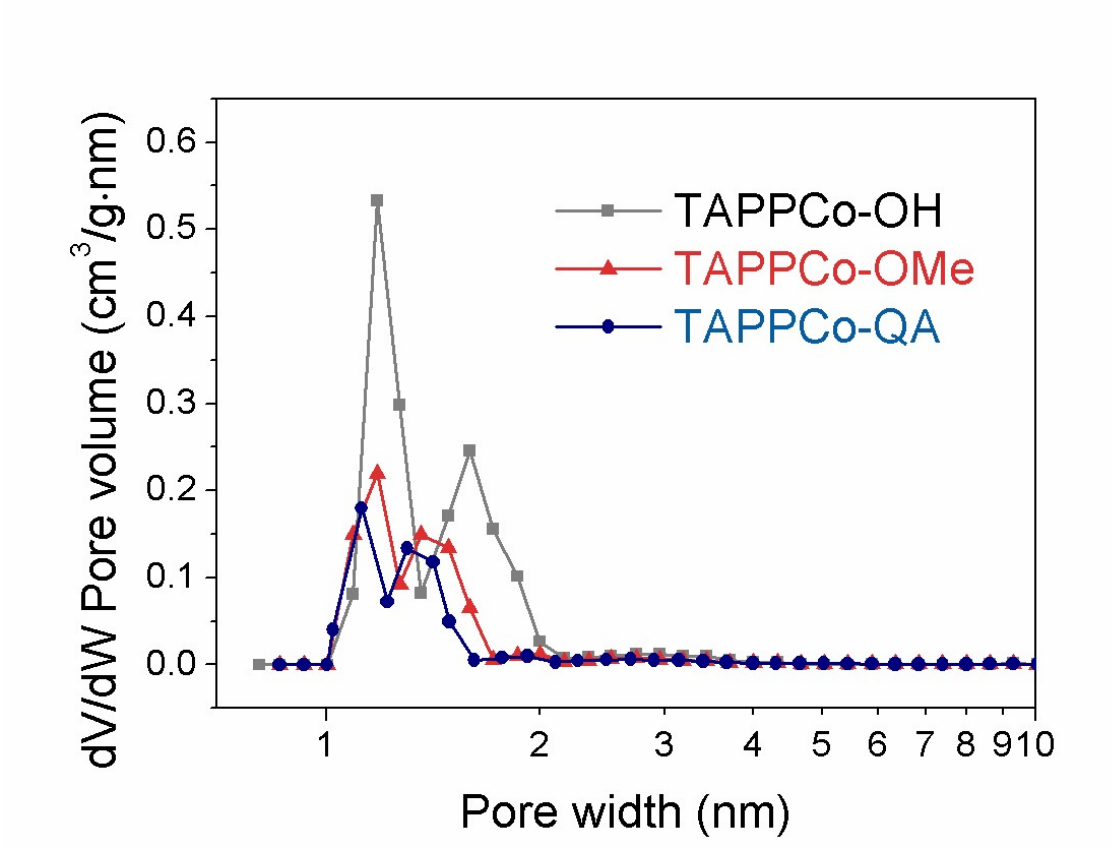

Fig. S7 Pore size distributions of the TAPPCo-OH COF, TAPPCo-OMe COF and TAPPCo-QA COF.

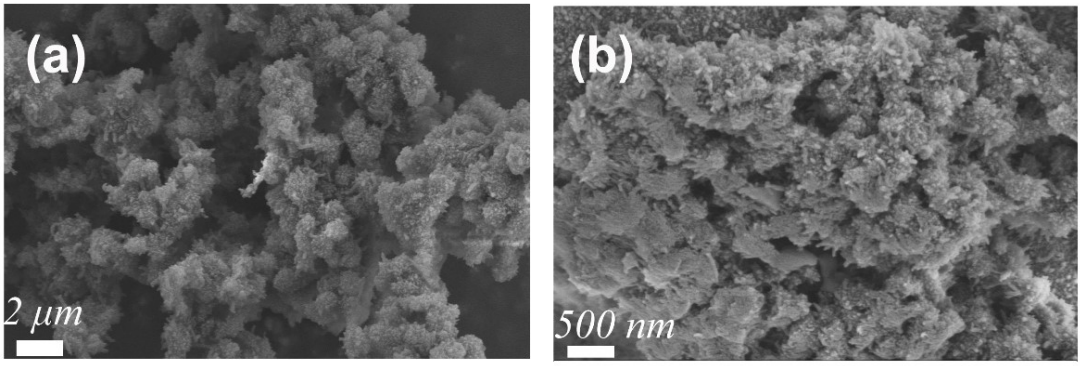

Fig. S8 SEM images of the TAPPCo-OH COF

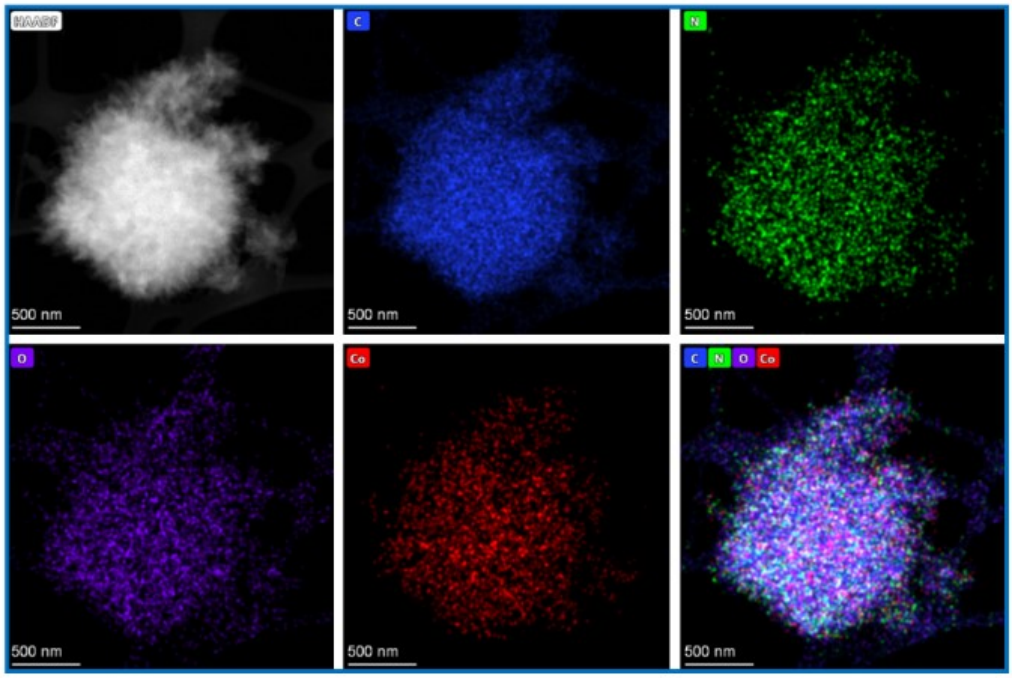

Fig. S9 The EDS elemental mapping of TAPPCo-QA

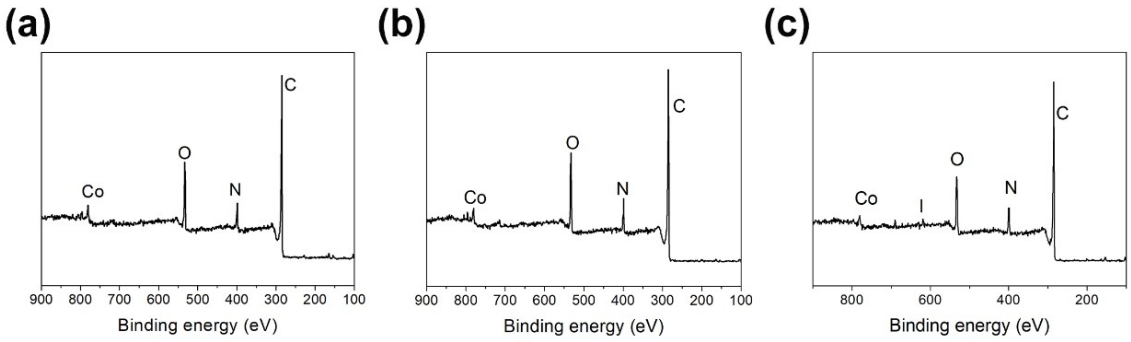

Fig. S10 XPS survey spectra of (a) TAPPCo-OH COF, (b) TAPPCo-OMe COF, and (c) TAPPCo-QA COF

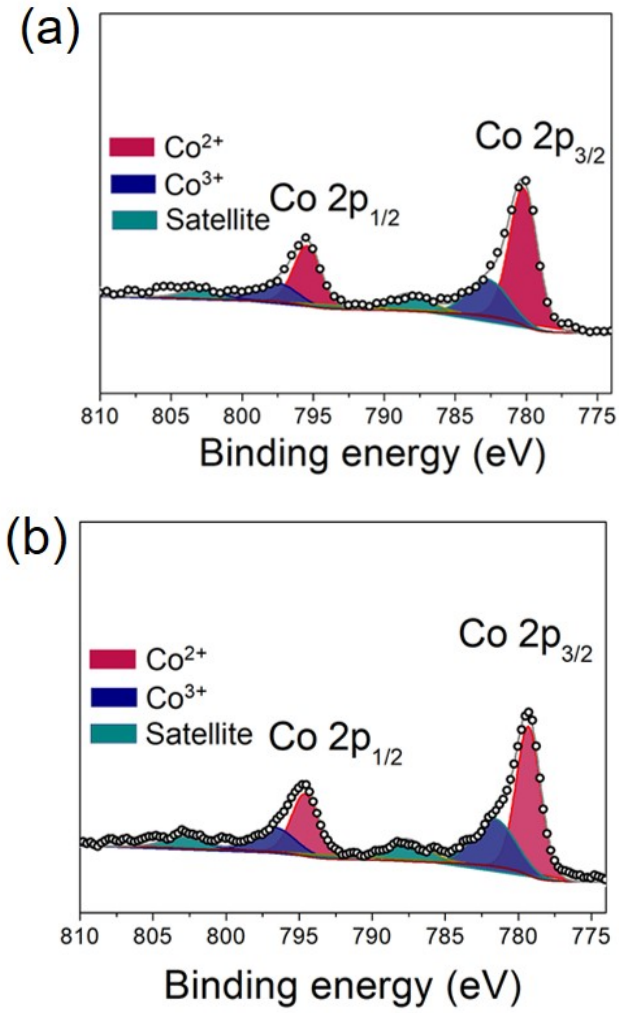

Fig. S11 High-resolution Co 2p XPS spectra of the (a) TAPPCo-OMe COF and (b) TAPPCo-OH COF

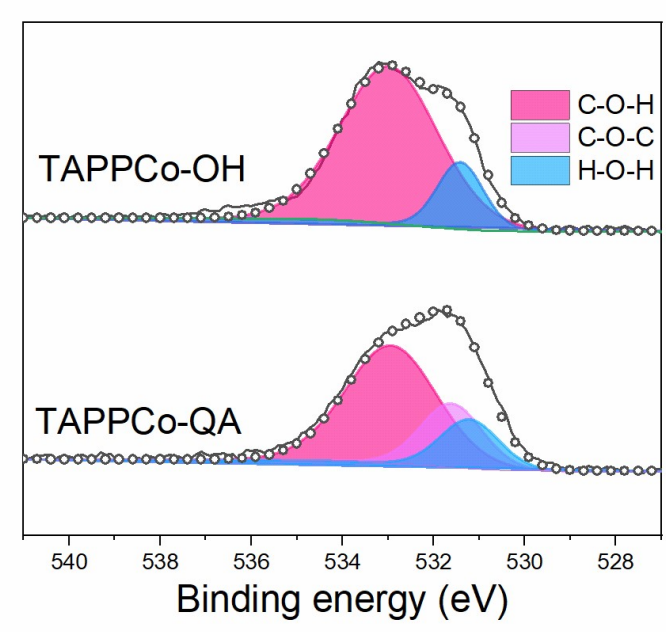

Fig. S12 High-resolution O 1s XPS spectra of TAPPCo-OH and TAPPCo-QA

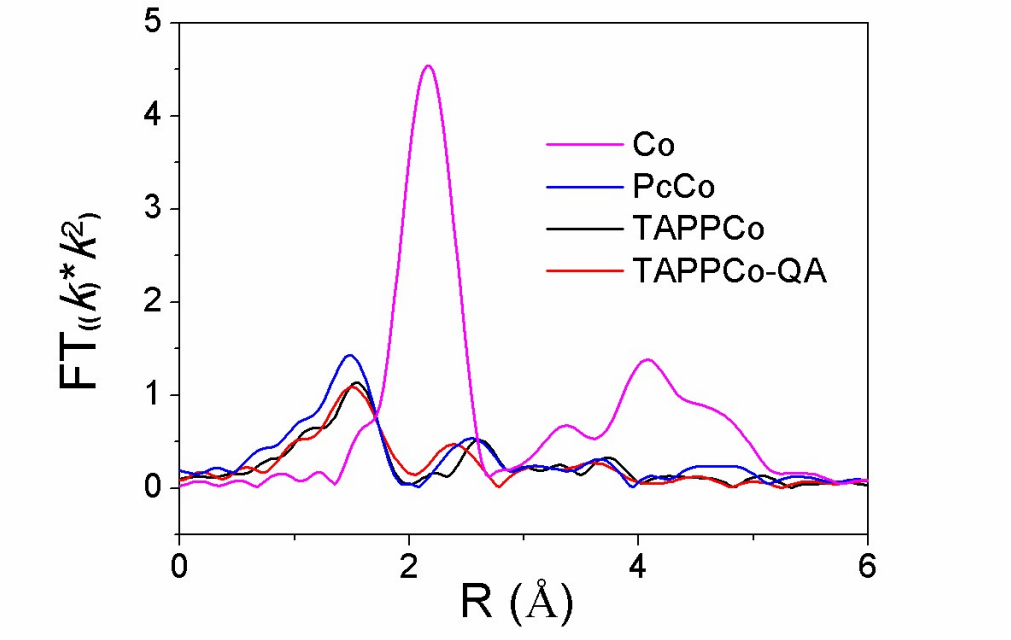

Fig. S13 Experimental Fourier transform of the Co K-edge data of Co, CoPc, TAPPCo and TAPPCo-QA.

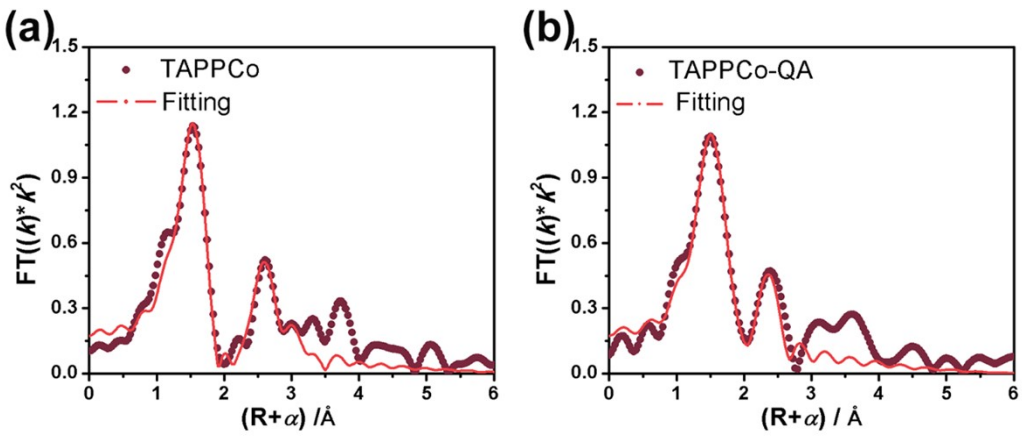

Fig. S14 Experimental and fitted Fourier transform of the Co K-edge data of (a) TAPPCo and (b) the TAPPCo-QA COF.

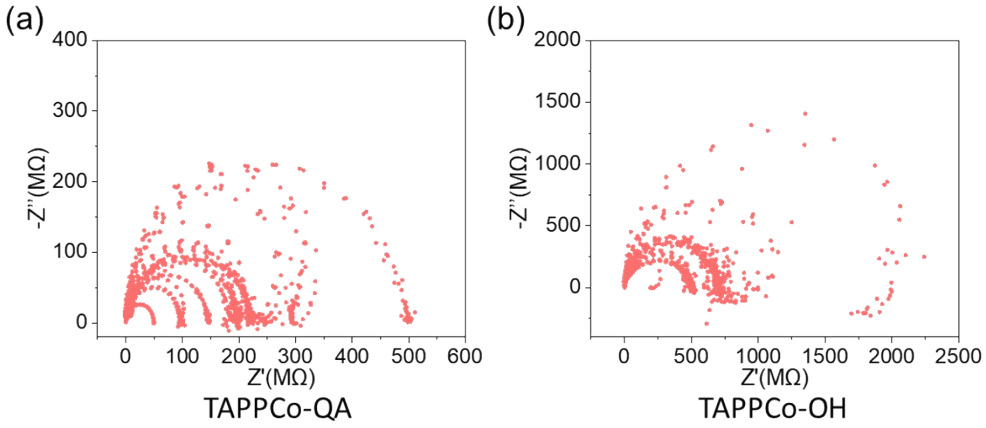

Fig. S15 Nyquist impedance plots of (a) TAPPCo-QA and (b) TAPPCo-OH. All AFM-EIS measurements were conducted at 25 °C with a relative humidity of 65%. Direct current (dc) bias: 2 V; amplitude of the alternating current (ac) excitation signal: 100 mV; and frequency range: 100 kHz~1 Hz.

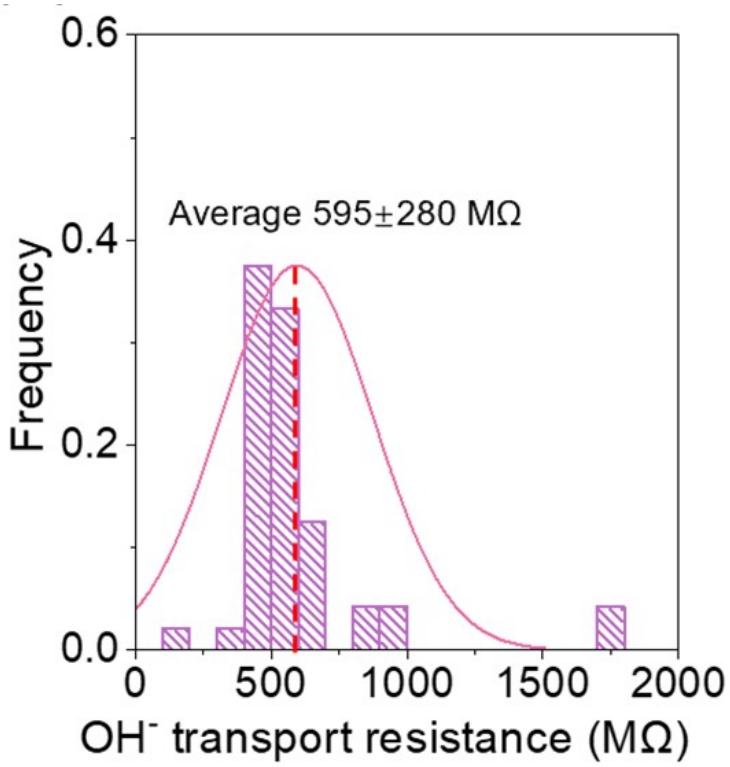

Fig. S16 Histogram of the local ion transport resistances of TAPPCo-OH.

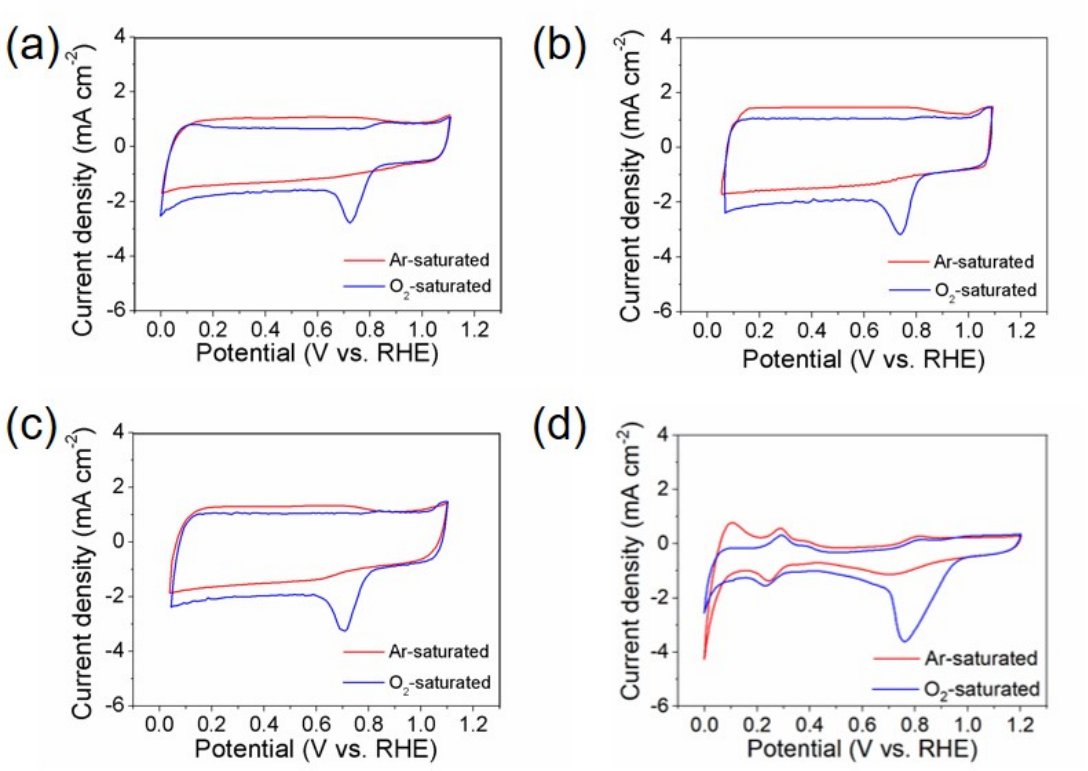

Fig. S17 CV curves of the (a) TAPPCo-OH COF, (b) TAPPCo-QA COF, (c) TAPPCo-OMe COF, (d) Pt/C in Ar-saturated and O_2-saturated 0.1 M KOH solution

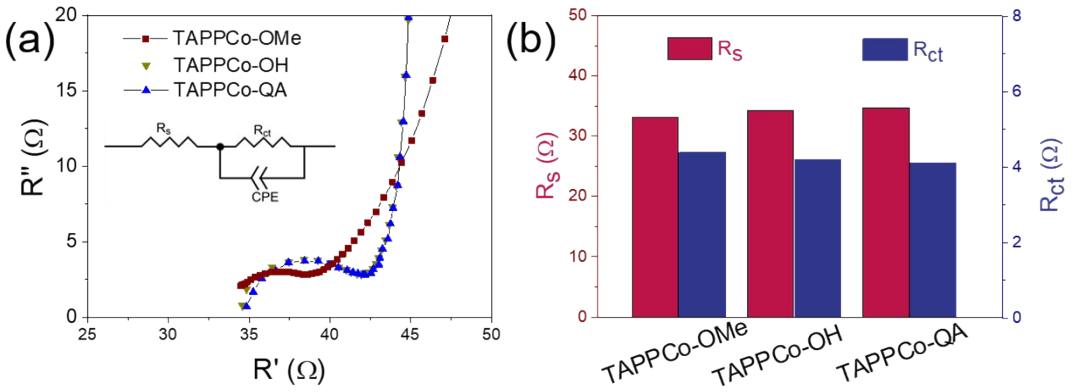

Fig. S18 (a) EIS curves of TAPPCo-OH, TAPPCo-QA and TAPPCo-OMe , (b) R_S and R_{ct} of TAPPCo-OH, TAPPCo-QA and TAPPCo-OMe

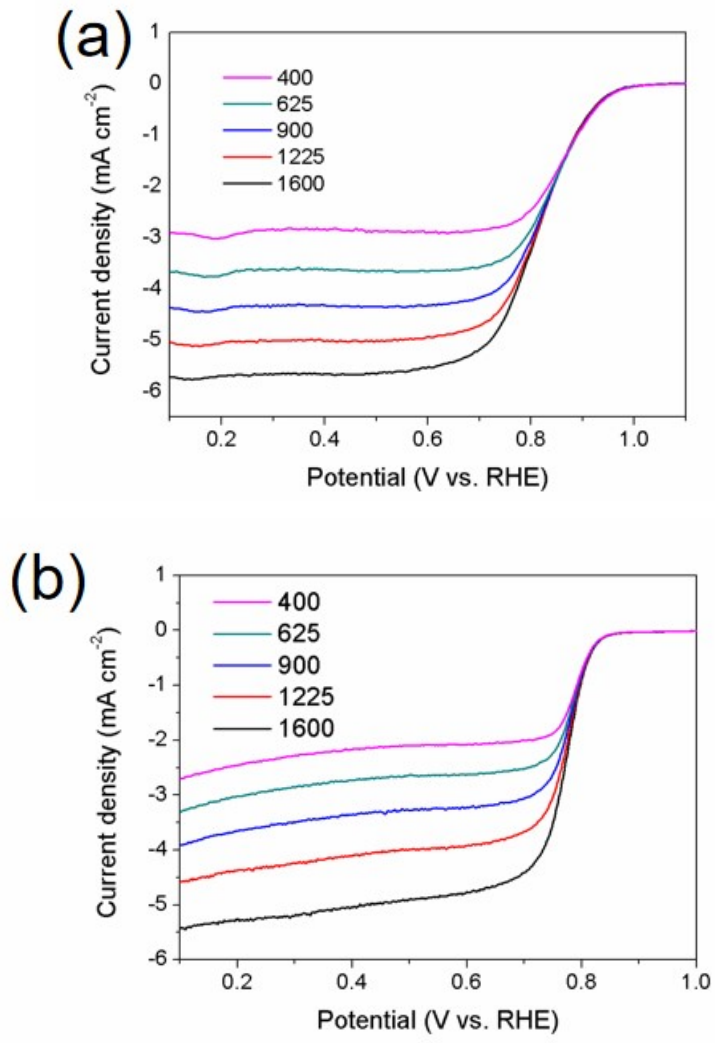

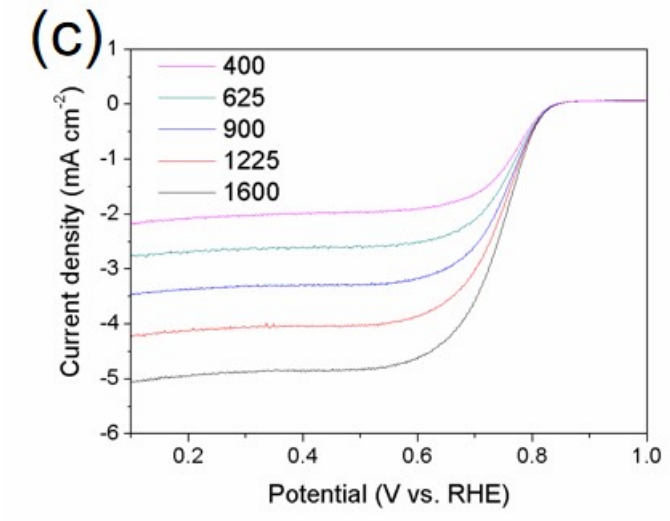

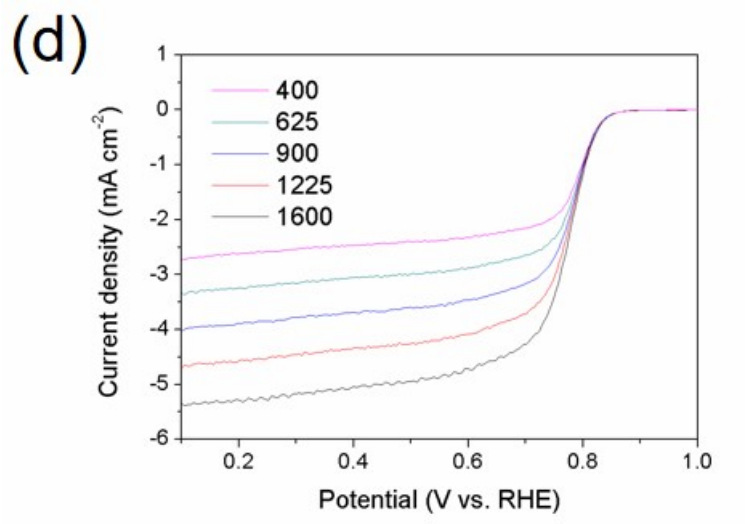

Fig. S19 ORR polarization curves of (a) Pt/C, (b) TAPPCo-QA, (c) TAPPCo-OMe and (d) TAPPCo-OH at different rotating speeds in a 0.1 M O_2-saturated KOH solution at a scan rate of 10 mV s^{-1}

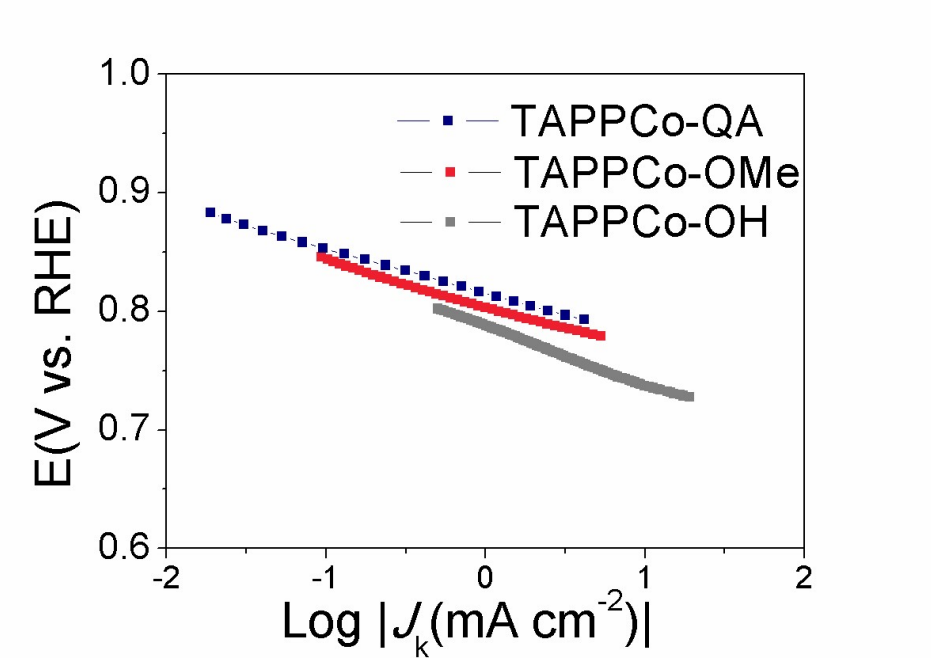

Fig. S20 Tafel curves of different catalysts at a rotating speed of 1600 rpm in a 0.1 M O_2-saturated KOH solution

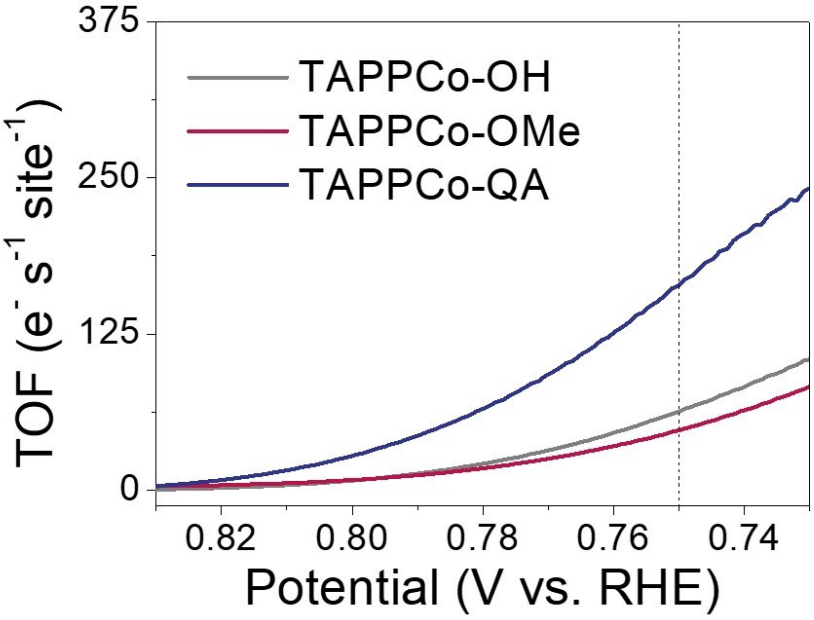

Fig. S21 TOF of the Co site in TAPPCo-OH, TAPPCo-OMe and TAPPCo-QA

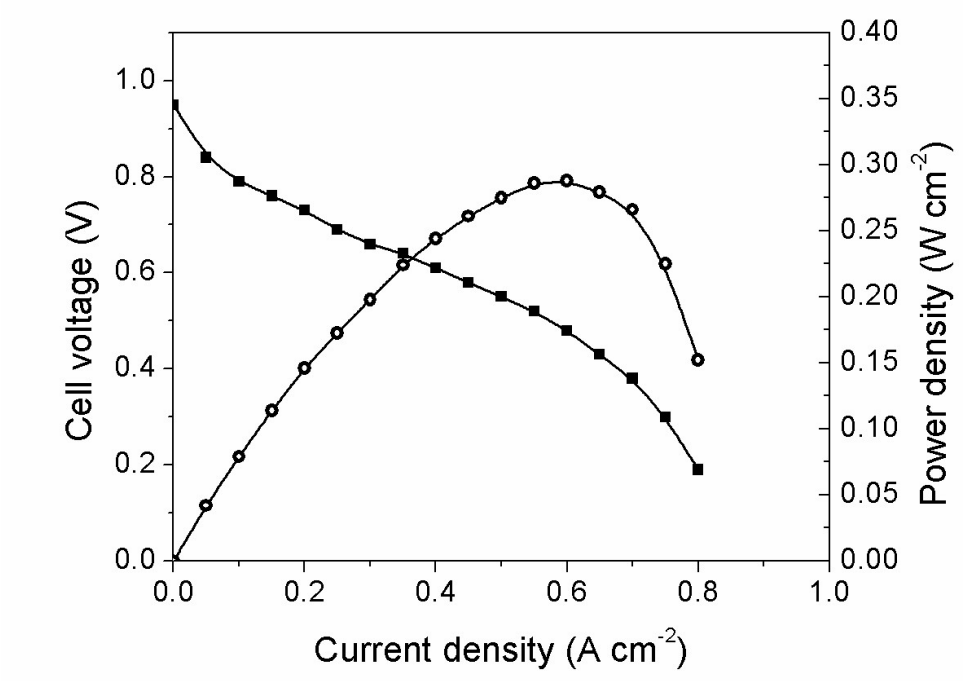

Fig. S22 AEMFC performance of the Pt/C (The loading of anodic PtRu/C catalyst is 1 $mg_{metal}\ cm^{-2}$; the loading of cathodic Pt/C catalyst is 1 $mg_{Pt}\ cm^{-2}$; Membrane: FAA-50; Temperature: 60℃; RH=75%; 500 mL min^{-1}, H_2/O_2)

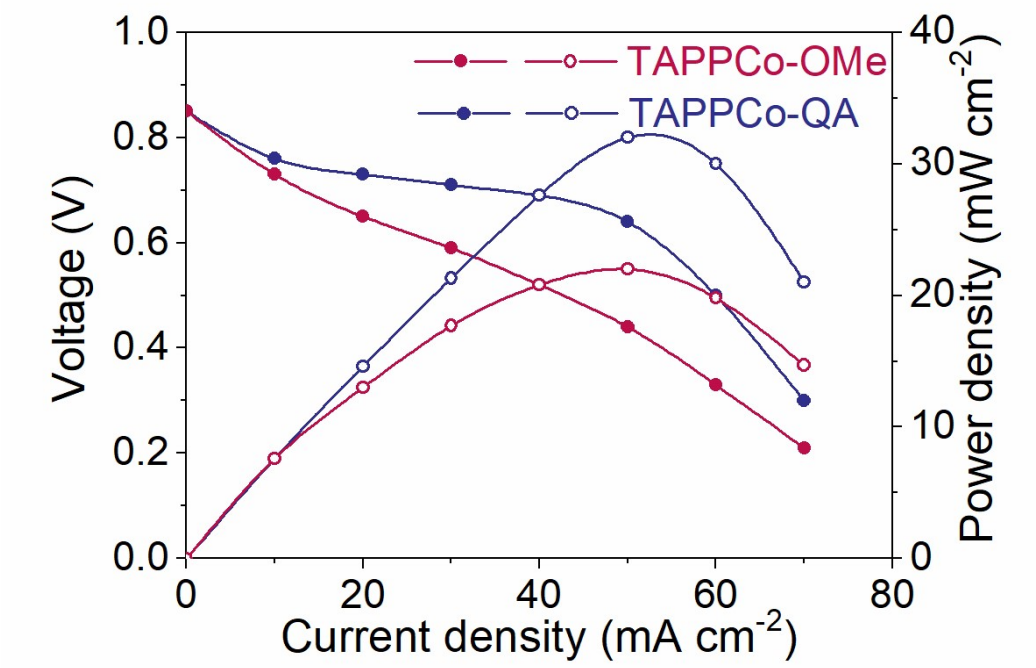

Fig. S23 AEMFC performance of the TAPPCo-OMe and TAPPCo-QA without ionomer in the cathode catalyst layer (The loading of anodic PtRu/C catalyst is 1 mg_{metal} cm^{-2}; The loading of cathodic TAPPCo-OMe/TAPPCo-QA catalysts is 3 mg cm^{-2}; Membrane: FAA-50; Temperature:60℃; RH=75%; 500 mL min^{-1}, H_2/O_2)

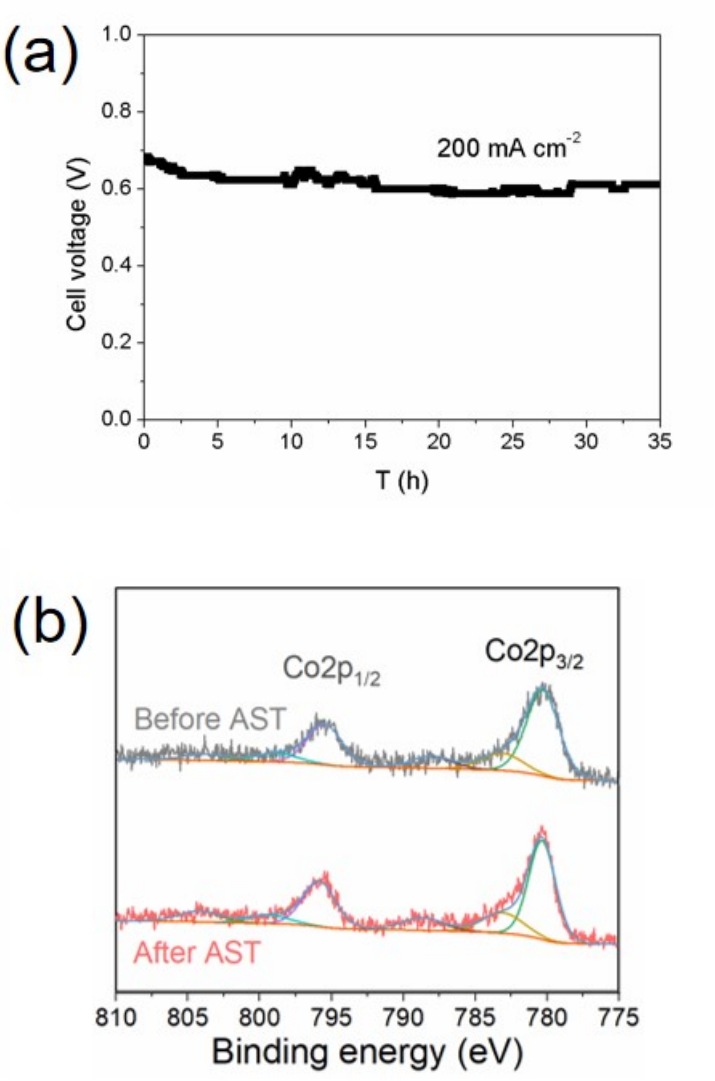

Fig. S24 (a) MEA stability test of TAPPCo-QA (The loading of anodic PtRu/C catalyst is 1 mg_{metal} cm^{-2}; The loading of cathodic TAPPCo-QA catalyst is 3 mg cm^{-2}; Membrane: FAA-50; Temperature: 60℃; RH=75% ; 500 mL min^{-1}, H_2/O_2); (b) Co 2p XPS spectra of the TAPPCo-QA COF before and after MEA stability measurements

Table S1. N and Co species ratios of TAPPCo-based COFs fitted from the high-resolution XPS N 1s and Co 3p spectra.

COFs	N	N			Co	Co	
	Content*	Pyrrolic	Imine	Quaternary	Content**	Co^{2+}	Co^{3+}
TAPPCo-OH	9.5%	45%	55%	--	5.5%	76%	24%
TAPPCo-OMe	9.3%	48%	52%	--	5.2%	79%	21%
TAPPCo-QA	8.9%	41%	43%	16%	4.8%	83%	17%

* The N content was obtained by the elemental analysis test.

** The Co content was obtained by the ICP test.

Table S2. K-edge absorption edge energy of Co, CoPc, TAPPCo and TAPPCo-QA

sample	Co	CoPc	TAPPCo	TAPPCo-QA
K-edge absorption energy(eV)	7709	7715.5	7713.5	7720.5

*The K-edge absorption energy (eV) takes the first maximum value of the derivative of the curve.

Table S3. EXAFS fitting results at the Co K-edge for TAPPCo and the TAPPCo-QA COF (S_0^2=0.72).

Sample	Path	CN	R / Å	σ^2 / Å^2	ΔE_0 / eV	R-factor
TAPPCo	Co-N	4.0(fixed)	1.95±0.01	0.002±0.001	8.0±1.6	0.020
	Co-C_1	8.0(fixed)	2.98±0.01	0.003±0.002		
TAPPCo-QA	Co-N	4.0±0.8	1.99±0.02	0.005±0.003	2.4±2.3	0.020
	Co-C	8.0±1.2	3.00±0.10	0.020±0.010		

[a] CN, the coordination number; R, the interatomic distance; σ^2, Debye-Waller factors; ΔE_0, the inner potential correction; R-factor: the goodness of fitting. These factor values were fixed based on the known structure of TAPPCo during EXAFS fitting.

Table S4. Numerical equivalent circuit fitting results of the local electrochemical impedance spectrum obtained from 50 randomly selected points on TAPPCo-QA.

Position	R_1 (Ω)	CPE_1-T ($F\ cm^{-2}s^{n-1}$)	CPE_1-P (n1)	R_2(Ω)	CPE_2-T ($F\ cm^{-2}s^{n-1}$)	CPE_2-P (n2)
1	20.1	1.597E-08	0.257	76.89	1.601E-07	0.658
2	0.8697	2.2437E-07	0.632	48.32	4.8738E-08	0.548
3	2.006	1.2555E-06	0.97052	194.2	3.0664E-07	0.543
4	92.12	2.5033E-06	0.9637	131.7	6.5808E-07	0.807
5	117.3	6.0368E-08	0.435	174.3	2.0427E-06	0.95346
6	2.822	1.2446E-06	0.97	193.3	4.0249E-07	0.489
7	2.879	1.2356E-06	0.96984	194.3	3.0002E-07	0.506
8	45.26	1.0054E-07	0.894	170.5	4.8762E-08	0.733
9	48.36	2.6654E-07	0.726	167.8	4.8418E-08	0.536
10	149.8	9.3662E-08	0.859	96.82	5.3173E-09	0.394
11	98.78	2.9991E-09	0.442	151.3	7.0127E-08	0.777
12	0.27052	3.0107E-08	0.446	48.94	3.3156E-07	0.528
13	4.991	1.3078E-06	0.96982	189.9	4.3789E-07	0.427
14	21.5	1.6174E-08	0.76	75.79	1.2826E-07	0.874
15	1.083	2.1623E-07	0.527	95.01	1.54E-08	0.42
16	8.176	9.4175E-08	0.709	186.7	3.2289E-07	0.872
17	29.97	2.8058E-07	1	166.9	1.9912E-08	0.462
18	87.55	4.2606E-07	0.99431	404.1	6.544E-06	1
19	23	4.6107E-07	0.98752	468.6	4.6147E-07	0.889
20	2.54	2.197E-07	1	94.53	3.7728E-07	0.716
21	31.25	3.0174E-07	0.99478	165.1	2.7683E-08	0.432
22	2.263	2.3039E-07	1	194.1	3.1476E-07	0.643
23	73.71	3.2097E-08	0.453	146	2.0665E-06	0.94929
24	74.31	2.9666E-08	0.462	147.1	1.9911E-06	0.95179
25	74.04	2.9495E-08	0.463	147.3	1.9962E-06	0.95158

26	76.58	7.7486E-08	0.332	226.2	2.3513E-06	0.94335
27	61.68	1.9009E-06	0.9907	164.1	7.7264E-07	0.99567
28	88.23	2.3663E-06	0.96393	135.3	6.667E-07	1
29	92.33	2.4601E-06	0.96599	131.7	6.5864E-07	1
30	108.4	8.1332E-08	0.391	185	2.4617E-06	0.93618
31	114.9	6.2167E-08	0.429	176.8	2.068E-06	0.95265
32	121	5.7742E-08	0.443	170.9	2.0088E-06	0.95444
33	111	6.4805E-08	0.422	181.4	2.0893E-06	0.95217
34	1.481	2.3926E-06	0.95485	144.6	3.3984E-06	1
35	1.655	2.2885E-06	0.95763	144.4	3.3195E-06	0.781
36	1.722	2.2519E-06	0.95876	144.4	3.4281E-06	0.876
37	1.548	2.2781E-06	0.9568	144.5	3.0344E-06	0.793
38	1.698	2.2734E-06	0.95729	144.4	3.2543E-06	0.582
39	9.426	4.6416E-07	0.98989	177.7	1.3855E-07	0.768
40	9.297	4.7276E-07	0.98788	177.7	1.3689E-07	0.572
41	8.94	4.6735E-07	0.98845	178.6	1.3266E-07	0.675
42	10.16	3.1355E-06	0.98937	211.5	2.44E-07	0.806
43	10.14	3.1571E-06	0.98848	211.7	2.3928E-07	0.707
44	9.976	3.2293E-06	0.98564	211.9	1.5967E-07	0.643
45	10.19	3.166E-06	0.98808	211.5	2.9411E-07	0.784
46	41.58	1.3201E-07	0.311	154.7	5.9169E-06	0.90807
47	41.79	1.3034E-07	0.312	154.3	5.9262E-06	0.90776
48	41.57	1.2904E-07	0.313	154.6	5.8844E-06	0.90827
49	41.46	1.2794E-07	0.313	154.9	5.8864E-06	0.90817
50	41.89	1.2882E-07	0.313	154.6	5.8723E-06	0.90829

* The equivalent circuit fitting process was conducted by using ZView software to obtain the local charge transfer resistances of TAPPCo-QA. All AFM-EIS measurements were conducted at 25 °C with a relative humidity of 65%. Direct current (dc) bias: 2 V; amplitude of the alternating current (ac) excitation signal: 100 mV; and frequency range: 100 kHz~1 Hz.

Table S5. Numerical equivalent circuit fitting results of the local electrochemical impedance spectrum obtained from 50 randomly selected points on TAPPCo-OH.

Position	R_1 (Ω)	CPE_1-T (F $cm^{-2}s^{n-1}$)	CPE_1-P (n1)	R_2(Ω)	CPE_2-T (F $cm^{-2}s^{n-1}$)	CPE_2-P (n2)
1	177.1	3.6097E-7	0.95508	1744	6.897E-8	0.784
2	98.95	1.0949E-7	1	853.3	1.5349E-8	0.831
3	90.92	1.0935E-7	0.864	947.8	1.3108E-8	0.837
4	257.1	2.3138E-6	0.87959	461.7	2.7243E-8	0.441
5	81.4	2.5987E-8	0.542	651.5	6.1202E-7	0.95815
6	209.2	3.8624E-7	0.94591	1748	5.6037E-8	0.713
7	127	5.7888E-8	0.454	594.4	9.624E-7	0.94899
8	140.8	3.9428E-8	0.486	579.6	9.8752E-7	0.94685
9	143.7	4.1558E-8	1.477	577	9.6829E-7	0.94863
10	130.6	3.1657E-8	0.479	571.7	6.5319E-7	0.95336
11	96.73	2.587E-8	0.524	620	6.4151E-7	0.95436
12	95.31	2.7407E-8	0.524	633.7	6.2521E-7	0.95625
13	103.7	3.1205E-8	0.499	609.8	6.5774E-7	0.9525
14	115.8	2.9219E-8	0.497	584.9	6.5503E-7	0.95295
15	168.4	4.9844E-8	0.409	555.5	7.1546E-7	0.94721
16	121.7	2.8107E-8	0.498	574.7	6.6911E-7	0.95138
17	110.5	3.6188E-8	0.481	624.1	6.511E-7	0.95382
18	284.2	7.4462E-7	0.98464	507.4	7.0736E-9	0.607
19	212.9	1.0983E-6	0.825	484.6	4.4778E-6	0.94162
20	24.47	1.9696E-6	0.803	671.2	2.9334E-6	0.97032
21	123.5	1.0837E-6	0.798	578.8	3.6255E-6	0.95883
22	129.2	1.0258E-6	0.809	567.5	3.5497E-6	0.95995
23	155.4	1.0975E-6	0.781	539.6	3.7917E-6	0.95572
24	142.2	1.0648E-6	0.796	551.7	3.6578E-6	0.95803
25	151	1.1988E-6	0.673	543.9	3.7785E-6	0.95615

26	192.4	1.2214E-6	0.744	501.9	4.202E-6	0.9495
27	164.7	1.103E-6	0.778	530.2	3.8298E-6	0.95514
28	124.6	1.0057E-6	0.814	571.7	3.521E-6	0.96049
29	56.35	3.3279E-8	0.892	439.7	3.0625E-7	0.706
30	81.08	1.1448E-6	0.96907	144.4	1.1073E-8	0.894
31	97.6	2.8526E-8	0.975	397	3.3087E-7	0.99967
32	91.34	2.5262E-8	0.998	403.6	3.1736E-7	0.801
33	83.31	2.4543E-8	0.911	411.4	3.1797E-7	0.901
34	148.4	1.1397E-7	0.944	804	8.2571E-9	0.702
35	44.02	2.5464E-7	0.884	445.1	4.0742E-7	0.98603
36	42.12	2.6018E-7	0.885	448.5	4.0977E-7	0.98524
37	37	2.2302E-7	0.102	454.3	3.941E-7	0.986
38	39.82	2.3245E-7	0.895	451.6	3.9307E-7	0.98797
39	42.75	2.4484E-7	0.888	450.6	4.1655E-7	0.98405
40	59.87	2.2863E-7	0.735	992	2.9146E-8	0.881
41	9.972	5.0885E-7	0.787	475.2	2.0018E-7	0.944
42	12.43	6.5986E-7	0.855	475.4	1.8029E-7	0.954
43	16.31	2.0638E-6	0.94737	475.4	1.3155E-7	0.997
44	43.64	2.4404E-7	0.792	459.7	5.3059E-7	0.98284
45	38.25	2.2998E-7	0.702	465.2	5.3038E-7	0.9793
46	40.34	2.4897E-7	0.793	463	5.2921E-7	0.98117
47	39.85	2.4065E-7	0.797	463.3	5.3472E-7	0.98026
48	40.28	2.2989E-7	0.899	462.8	5.3557E-7	0.98059
49	57.85	2.2503E-7	0.940	852	2.9847E-8	0.985
50	104.6	1.1094E-6	0.754	561.8	3.423E-6	0.86248

*The equivalent circuit fitting process was conducted by using ZView software to obtain the local charge transfer resistances of TAPPCo-OH. All AFM-EIS measurements were conducted at 25 °C with a relative humidity of 65%. Direct current (dc) bias: 2 V; amplitude of the alternating current (ac) excitation signal: 100 mV; and frequency range: 100 kHz~1 Hz.

Table S6. Comparison of the AEMFC performance of various macrocycle-derived electrocatalysts in the literature.

Catalyst	Types of Catalysts	Macrocycle	Cathode loading (mg cm^{-2})	T (°C)	P_{max} (mW cm^{-2})	Ref
CoPc/XC-72	molecular	CoPc	2	50	105	2
CoPc/C	molecular	CoPc	3	RT	12.6	3
FePc/MWCNT	molecular	FePc	0.6	45	60	4
CoPc/MWCNT	molecular	CoPc	0.6	45	100	4
$CoFeN_x$/C	pyrolysis	hemin CoTMPP	2.5	60	37	5
CNT/PC	pyrolysis	FeTPP	2	80	380	6
FePc/C	pyrolysis	FePc	1	55	120	7
CS_FePc_450	pyrolysis	FePc	1	50	160	8
FeCo/XC-72	pyrolysis	FePc	1	50	178	9
FeCo/MNT	pyrolysis	FePc	1		182	10
CDC/CNT	pyrolysis	CoPc	0.7 ± 0.15	60	473	11
FePc-KCB	molecular	FePc	1	50	108	12
NPMC	molecular	CoPc	2	60	232	13
pyrolysed KB/FePc	pyrolysis	FePc	2.0 ± 0.2	60	186	14
HT800-FeP	pyrolysis	FeTPP	1.25	80	580	15
C@PVI-(DFTPP)Fe-800	pyrolysis	FeTPP	2	60	104	16

MWCNT/CoPc	molecular	CoPc	-	RT	182[a]	[17]
Zn/Fe_{SA}-PC/950/NH3	pyrolysis	FeTPP[b]	3	60	352	[18]
PF-TMPPCo	molecular	CoTMPP	0.9 μg_{Co}	60	226	[19]

[a)] Performance of an alkaline glucose/O_2 fuel cell with 0.5 M KOH.

[b)] Fe-porphyrin, in the hemoglobin of pig blood.

References:

1. S. Lin, C. S. Diercks, Y.-B. Zhang, N. Kornienko, E. M. Nichols, Y. Zhao, A. R. Paris, D. Kim, P. Yang, O. M. Yaghi and C. J. Chang, *Science*, 2015, **349**, 1208-1213.
2. J. Guo, H. He, D. Chu and R. Chen, *Electrocatalysis*, 2012, **3**, 252-264.
3. T. Zhu, X. Qing, P. Xu, Y. Song and J. Qiao, *ECS Transactions*, 2015, **66**, 105-110.
4. I. Kruusenberg, L. Matisen, Q. Shah, A. M. Kannan and K. Tammeveski, *International Journal of Hydrogen Energy*, 2012, **37**, 4406-4412.
5. R. Jiang and D. Chu, *Journal of Power Sources*, 2014, **245**, 352-361.
6. Y. J. Sa, D.-J. Seo, J. Woo, J. T. Lim, J. Y. Cheon, S. Y. Yang, J. M. Lee, D. Kang, T. J. Shin, H. S. Shin, H. Y. Jeong, C. S. Kim, M. G. Kim, T.-Y. Kim and S. H. Joo, *Journal of the American Chemical Society*, 2016, **138**, 15046-15056.
7. H. A. Miller, M. Bellini, W. Oberhauser, X. Deng, H. Chen, Q. He, M. Passaponti, M. Innocenti, R. Yang, F. Sun, Z. Jiang and F. Vizza, *Physical Chemistry Chemical Physics*, 2016, **18**, 33142-33151.
8. D. Y. Chung, M. J. Kim, N. Kang, J. M. Yoo, H. Shin, O.-H. Kim and Y.-E. Sung, *Chemistry of Materials*, 2017, **29**, 2890-2898.
9. O. V. Korchagin, V. A. Bogdanovskaya, M. R. Tarasevich, A. V. Kuzov, G. V.

Zhutaeva, M. V. Radina, V. T. Novikov and V. V. Zharikov, *Catalysis in Industry*, 2016, **8**, 265-273.

10. L. Osmieri, R. Escudero-Cid, A. H. A. Monteverde Videla, P. Ocón and S. Specchia, *Renewable Energy*, 2018, **115**, 226-237.
11. R. Praats, M. Käärik, A. Kikas, V. Kisand, J. Aruväli, P. Paiste, M. Merisalu, A. Sarapuu, J. Leis, V. Sammelselg, J. C. Douglin, D. R. Dekel and K. Tammeveski, *Journal of Solid State Electrochemistry*, 2021, **25**, 57-71.
12. J. Yang, J. Tao, T. Isomura, H. Yanagi, I. Moriguchi and N. Nakashima, *Carbon*, 2019, **145**, 565-571.
13. M. Mooste, T. Tkesheliadze, J. Kozlova, A. Kikas, V. Kisand, A. Treshchalov, A. Tamm, J. Aruväli, J. H. Zagal, A. M. Kannan and K. Tammeveski, *International Journal of Hydrogen Energy*, 2021, **46**, 4365-4377.
14. R. Praats, M. Käärik, A. Kikas, V. Kisand, J. Aruväli, P. Paiste, M. Merisalu, J. Leis, V. Sammelselg, J. H. Zagal, S. Holdcroft, N. Nakashima and K. Tammeveski, *Electrochimica Acta*, 2020, **334**, 135575.
15. N. Zion, J. C. Douglin, D. A. Cullen, P. Zelenay, D. R. Dekel and L. Elbaz, *Advanced Functional Materials*, 2021, **31**, 2100963.
16. Y.-M. Zhao, P.-C. Zhang, C. Xu, X.-Y. Zhou, L.-M. Liao, P.-J. Wei, E. Liu, H. Chen, Q. He and J.-G. Liu, *ACS Applied Materials & Interfaces*, 2020, **12**, 17334-17342.
17. K. Elouarzaki, A. Le Goff, M. Holzinger, J. Thery and S. Cosnier, *Journal of the American Chemical Society*, 2012, **134**, 14078-14085.
18. H. S. Kim, J. Lee, J.-H. Jang, H. Jin, V. K. Paidi, S.-H. Lee, K.-S. Lee, P. Kim and S. J. Yoo, *Applied Surface Science*, 2021, **563**, 150208.
19. R. Ren, X. Wang, H. Chen, H. A. Miller, I. Salam, J. R. Varcoe, L. Wu, Y. Chen, H.-G. Liao, E. Liu, F. Bartoli, F. Vizza, Q. Jia and Q. He, *Angewandte Chemie International Edition*, 2021, **60**, 4049-4054.